

SCIENTIFIC REPORTS



OPEN

Three-dimensionally Ordered Macroporous Structure Enabled Nanothermite Membrane of $\text{Mn}_2\text{O}_3/\text{Al}$

Received: 26 November 2015

Accepted: 18 February 2016

Published: 03 March 2016

Guoqiang Zheng¹, Wenchao Zhang¹, Ruiqi Shen¹, Jiahai Ye¹, Zhichun Qin¹ & Yimin Chao²

Mn_2O_3 has been selected to realize nanothermite membrane for the first time in the literature. $\text{Mn}_2\text{O}_3/\text{Al}$ nanothermite has been synthesized by magnetron sputtering a layer of Al film onto three-dimensionally ordered macroporous (3DOM) Mn_2O_3 skeleton. The energy release is significantly enhanced owing to the unusual 3DOM structure, which ensures Al and Mn_2O_3 to integrate compactly in nanoscale and greatly increase effective contact area. The morphology and DSC curve of the nanothermite membrane have been investigated at various aluminizing times. At the optimized aluminizing time of 30 min, energy release reaches a maximum of $2.09 \text{ kJ} \cdot \text{g}^{-1}$, where the Al layer thickness plays a decisive role in the total energy release. This method possesses advantages of high compatibility with MEMS and can be applied to other nanothermite systems easily, which will make great contribution to little-known nanothermite research.

In recent years, the demand for miniaturization and integration of power generator has significantly increased in microelectromechanical system (MEMS). Although chemical battery technologies have been greatly developed, the energy density is still relatively low. It is impossible to attain large energy release from the micro-scale batteries¹. It is critical to find a new class of highly efficient materials for MEMS. Nanoenergetic materials (nEMs) are supposed to be one key to the great advance in power generator owing to their high energy density, high compatibility, and the improved microfabrication processes such as photolithography, thin film deposition and doping^{2,3}.

Nanothermite, also termed metastable intermolecular composites (MIC), is a typical class of nEMs. An MIC generally consists of fuel (such as Al, Mg) and a variety of metal oxides (e.g. CuO , Fe_2O_3 , MoO_3 , Bi_2O_3 , NiO). Under the stimulus of flame, laser pulse, current or heating, an oxidation-reduction reaction breaks out and releases a large amount of energy. Owing to shorter mass transfer distance and larger contact area, MICs show better performance in energy release, ignition delay time and reaction rate compared to their bulk or micro counterparts^{3–7}, and have also revealed promising applications in many fields including microinitiators, gas generators, microheaters and microthrusters^{8–13}. In the past two decades, various techniques have been developed to prepare MICs, such as physical mixing^{14–16}, sol-gel/aero-gel^{17,18}, molecular self-assembly^{19–21}, physical vapor deposition (PVD)^{22–25}, and high-energy ball milling¹³. Each method has its own advantages to meet different experimental conditions and applications. Among all kind of methods, PVD and its ramifications are shown to be the most compatible with MEMS.

In 2003, Blobaum *et al.* demonstrated a sputtering method for deposition of CuO_x/Al multilayer foils, and investigated the reaction path and growth kinetics in CuO_x/Al thermite reaction. Their results showed CuO_x/Al foils could react in a highly exothermic manner^{26,27}. This work opened the perspective for application of PVD in thermite films preparation. Afterwards, Bahrami *et al.* prepared multilayered CuO/Al thermites in nanoscale and microscale using magnetron sputtering. After the comparison of the thermite reactions in different structures, the results confirmed that nanostructures made contribution to faster burning rate and higher energy release²⁸. Zhu *et al.* obtained similar conclusion by comparing MoO_x/Al multilayer nanofilms with different ratios of bilayer thicknesses²⁹. This multilayer approach has the advantages of controllable ratio of reactants and compatibility with MEMS, but the fabrication process is expensive and requires high performance instrument. Moreover,

¹School of Chemical Engineering, Nanjing University of Science and Technology, Nanjing, 210094, China. ²School of Chemistry, University of East Anglia, Norwich, NR47TJ, United Kingdom. Correspondence and requests for materials should be addressed to W.Z. (email: zhangwenchao303@aliyun.com) or Y.C. (email: y.chao@uea.ac.uk)

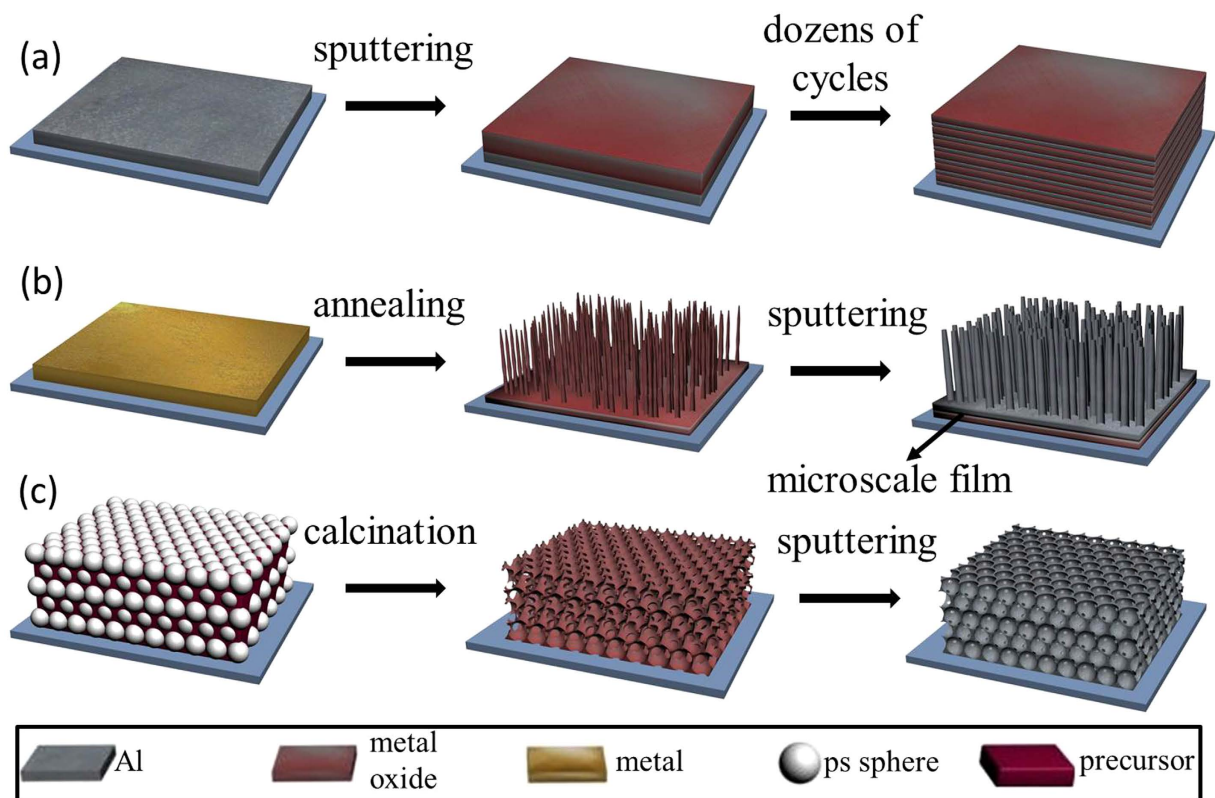


Figure 1. Comparison of three different fabrication methods of nanothermite: (a) multilayer films, (b) NWs core/shell structure, (c) 3DOM nanothermite membrane.

nanoscale multilayer films with a certain thickness generally require dozens of modulation cycles, which is time consuming and discommodious. Recently, one-dimensional nanowires (NWs) were developed to prepare core/shell nanothermite, in which NWs were synthesized by thermally annealing metal film followed by deposition of Al shell^{5,30}. Such core/shell structures can increase contact area and lower activation energy effectively. However, there are some concerns over this route: the length of NWs is not arbitrary; only a small fraction of metal oxide is included in NWs while most of them are still in the form of original film that appears in microscale. These limitations have a negative impact on the energy release and reaction rate²⁴. In addition, just few types of nanothermite have been prepared by the aforementioned two approaches.

Inspired by these two approaches above, in order to produce well-defined nanothermites, a novel 3DOM method has been developed in our lab, in which, the 3DOM metal oxide framework is prepared using inverse template method followed by depositing a layer of Al film using magnetron sputtering³¹. The distinct 3DOM structure guarantees the compact combination of fuel and oxidizer in nanoscale and enlarges the effective contact area significantly. This approach is very easy for popularization and mass production. The feasibility of this method has been preliminarily verified in previous work through $\text{Fe}_2\text{O}_3/\text{Al}$ system^{31,32}, and the energy release is significantly larger than those previously reported from other structures^{17,21,33}. Notably, most of metal oxides have been successfully formed into 3DOM structure^{34,35}. Figure 1 shows the comparison of three different fabrication methods of nanothermite that are reviewed above. In this paper, Mn_2O_3 has been selected as an oxidant to prepare nanothermite, which is the first attempt in the literature. Through the investigation of different aluminizing time or molar ratio effects on the morphology and energy release, the reaction path of $\text{Mn}_2\text{O}_3/\text{Al}$ nanothermite is widely discussed.

Results and Discussion

Phase Analysis. The phase of the crystalline components is identified by Powder X-ray diffraction (XRD) characterization. As shown in Fig. 2a XRD pattern of 3DOM Mn_2O_3 skeleton exhibits a strong peak at 32.95° , and some weak peaks at 23.13° , 38.23° and 55.19° , just similar to the purchased Mn_2O_3 nanoparticle in Fig. 2b, corresponding to planes (222), (211), (400) and (440) of bixbyite $\alpha\text{-Mn}_2\text{O}_3$ (JCPDS 41-1442), respectively. Figure 2c shows XRD pattern of 3DOM $\text{Mn}_2\text{O}_3/\text{Al}$ composite membrane. As expected, the diffraction peaks of Al are observed at 38.47° , 44.74° and 65.13° , corresponding to planes (111), (200), and (220) of Al. Simultaneously, the characteristic peaks of bixbyite Mn_2O_3 are kept in the same places without impure peaks, which reveals that phase transformation of Mn_2O_3 is avoided and the oxidation-reduction reaction between Al and Mn_2O_3 has not happened. These advantages are owing to the high-vacuum and the sustained low temperature during the aluminizing process. Over the $\text{Mn}_2\text{O}_3/\text{Al}$ nanoparticle composites (NPC) sample, XRD pattern also indicates good crystallinities of Al and Mn_2O_3 after grinding with care.

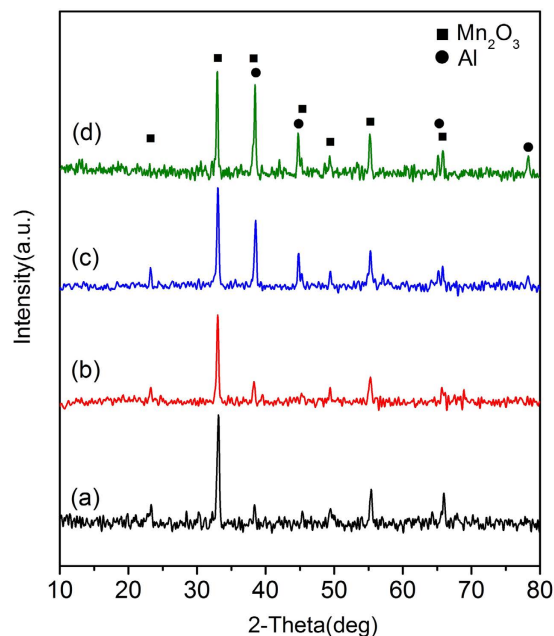


Figure 2. XRD patterns of (a) 3DOM Mn_2O_3 skeleton, (b) Mn_2O_3 nanoparticle, (c) 3DOM $\text{Mn}_2\text{O}_3/\text{Al}$ membrane, (d) $\text{Mn}_2\text{O}_3/\text{Al}$ nanoparticle composites.

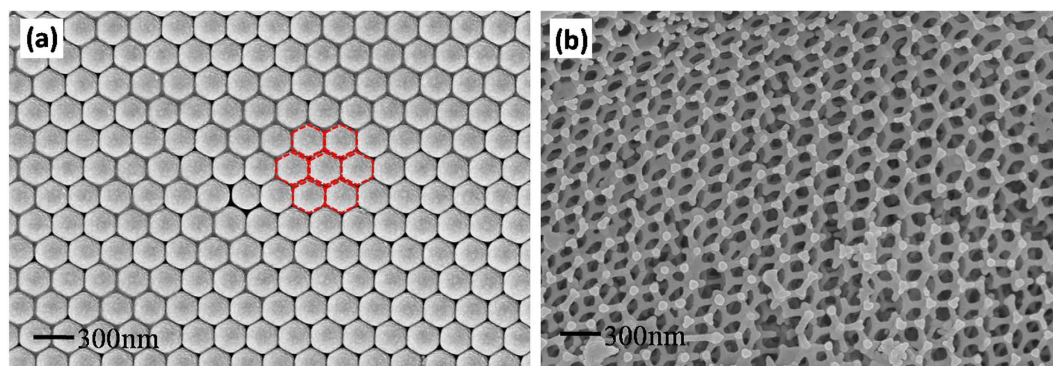


Figure 3. SEM images of (a) PS colloidal crystal template, (b) 3DOM Mn_2O_3 skeleton.

Morphology Characterization. Scanning electron microscope (SEM) images of polystyrene (PS) colloidal crystal template (CCT) prepared by vertical deposition are shown in Fig. 3a. The monodispersed PS spheres are with bright surface and assembled into hexagonally-close packed structure which has been proved to be one of the most stable arrangements on thermodynamics³⁶. Each sphere is surrounded by another six with uniform size and their planes oriented parallel to the surface of the microslide substrate, see red dash lines in Fig. 3a. The average diameter of the regular PS spheres is approximately 270 nm. Figure 3b shows the distinct 3DOM Mn_2O_3 structure, a high quality inverse replica of the template. Interconnected and ordered macroporous structure is observed after PS spheres are removed. A “honeycomb” structure is constituted by well-ordered air spheres and metal oxides walls in three dimensions with a thickness of 48 nm, and several layers within the skeleton are still visible in the surface image. The pore size is about 220 nm which corresponds to a pore shrinkage rate of approximately 18.5% compared with the original PS sphere. Some point defects and line defects are visible in the image. This is due to incomplete filling of the precursor and the transformation of the CCT during the calcination. Even so, we can consider that the integrity and consistency of the Mn_2O_3 skeleton are still maintained.

Figure 4 shows SEM images from $\text{Mn}_2\text{O}_3/\text{Al}$ membrane with three different aluminizing times and a typical $\text{Mn}_2\text{O}_3/\text{Al}$ nanoparticle composite. From surface view in Fig. 4a–c, one can see the rigid strength of the Mn_2O_3 skeleton is strong enough to support the deposited Al, and there is no fracture or collapse phenomenon. With aluminizing time increasing, the coated layer on the Mn_2O_3 wall is getting thicker, and the pore size is reduced. Figure 4a shows that wall thickness increases from the initial 48 nm to 86 nm because of deposition of Al, and increases further to 140 nm in Fig. 4b. When aluminizing time is increased to 30 min, only the wall trace can be seen dimly, and the pores are entirely filled. The same conclusion can be reached from the cross-section view of

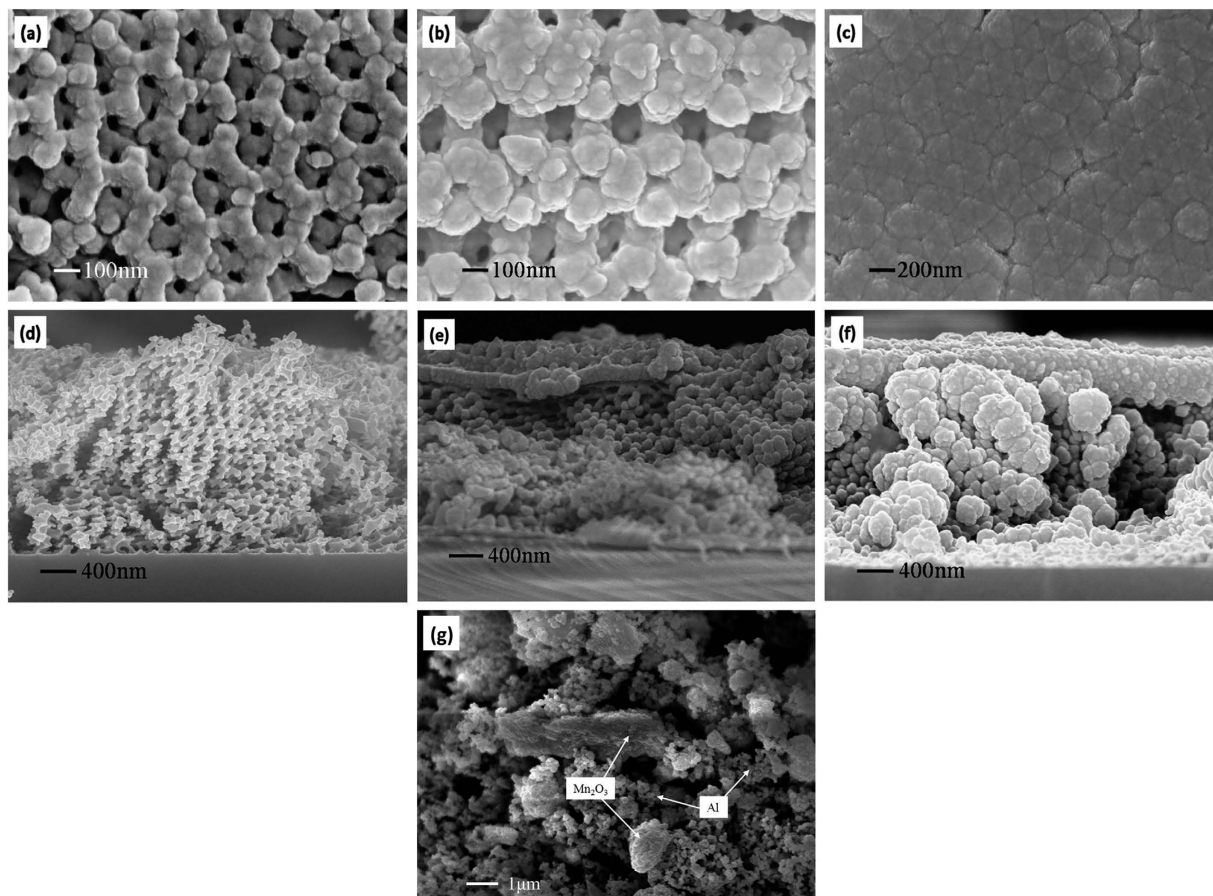


Figure 4. SEM images of Mn₂O₃/Al membrane with different aluminizing time of Al: (a,d) 10 min, (b,e) 20 min, (c,f) 30 min; (a–c) surface view and (d–f) cross-section view. (g) a typical Mn₂O₃/Al nanoparticle composite.

the samples in Fig. 4d–f, which reveal face-centered cubic (FCC) structure in three-dimensional view. The whole thickness of the composite membrane is about 2.6 μm.

For comparison, Fig. 4g shows the SEM image of Mn₂O₃/Al NPC. Mn₂O₃ particles are in the form of irregular morphology in nanoscales or macroscales, and the spherical Al particles are distributed among the Mn₂O₃ particles. One can see that Mn₂O₃ particles are severely agglomerated due to the high surface energy, and the dispersion homogeneity of Mn₂O₃/Al NPC is significantly lower than 3DOM Mn₂O₃/Al membrane. Furthermore, the cross-section view also has proved that Al is not only deposited on the surface, but presented in the interior of the Mn₂O₃ inverse template, see further discussion in the next section with X-ray photoelectron spectroscopy (XPS) results. In order to further exam the morphology of the Mn₂O₃/Al membrane, transmission electron microscope (TEM) images on cross section of Mn₂O₃/Al membrane with aluminizing time of 20 min are showed in Fig. 5. One can see Al is coated on 3DOM Mn₂O₃ skeleton to form a core/shell structure, and the nanothermite membrane can be viewed as an assembly of multiple nanothermite units, which are in agreement with the results obtained by SEM. Since Al is coated on Mn₂O₃ uniformly and connected with the skeleton closely both on the surface and inside the structure, one can expect the significantly enhanced effective contact area and improved reactivity.

Elemental Analysis. Energy dispersive spectrum (EDS) is used to obtain a further insight into the aluminizing time on the influence of the elemental ratio. Figure 6 shows the EDS spectra of the Mn₂O₃/Al membranes with corresponding SEM images. Al and Mn peaks are observed in the spectra, accompanying with some impurity peaks that should be ignored, such as Au and Si. Au is from the layer deposited onto samples prior to the SEM measurement in order to increase the electric conductivity, while Si signal is from the quartz substrate. It is visualized that the percentages of Al peaks are gradually increased exactly as shown in SEM images, see EDS elemental mapping in Fig. S1 in supporting information.

The atomic percentages of the element (%) are obtained by integration of the peak areas, and molar ratio of Al to Mn₂O₃ is then calculated, respectively. Due to the presence of impurities, only Al and Mn are taken into account, see Table 1. The results show that the molar ratio of Al to Mn₂O₃ increases gradually with the increasing of aluminizing time, and they are linearly related because of the constant deposition rate of Al. Since the quantity analysis relies heavily upon the homogeneity of the samples, this is an indicative estimation in quantitation. One can see the molar ratio of Al to Mn₂O₃ is slightly larger than the stoichiometric value of the exothermic self-propagating reaction between Al and Mn₂O₃ when the aluminizing time is added to 30 min.

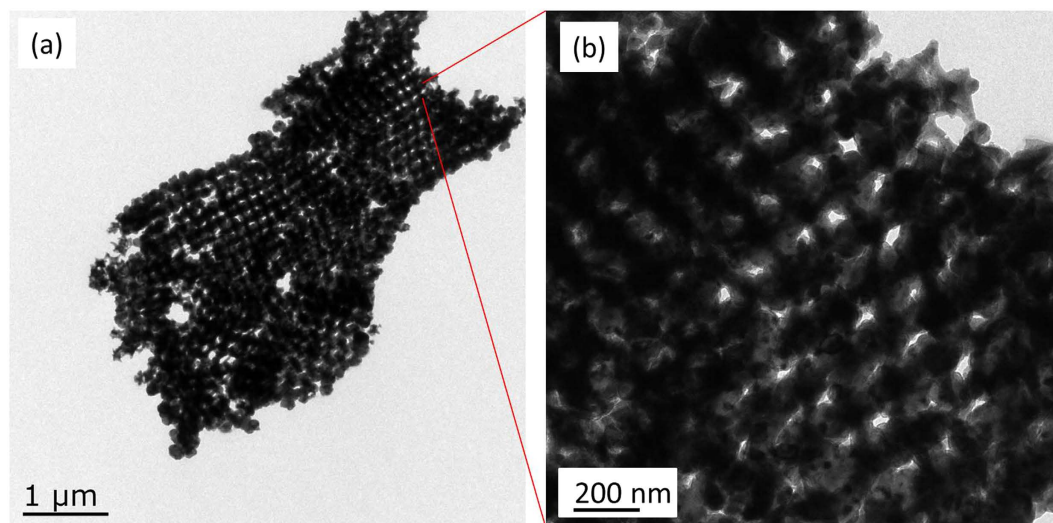


Figure 5. TEM images of Mn_2O_3/Al membrane with aluminizing time of 20 min.

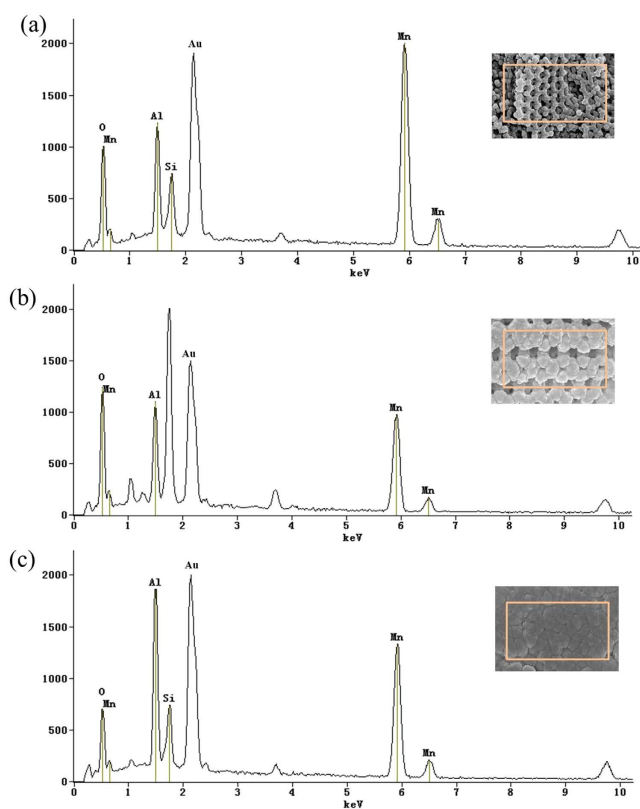


Figure 6. EDS spectrums of the Mn_2O_3/Al membrane with different aluminizing time. (a) 10 min, (b) 20 min, (c) 30 min.

aluminizing time (min)	Atomic percentage of the elements (%)		Molar ratio of Al to Mn_2O_3
	Al	Mn	
10	26.74	73.26	0.73
20	45.43	54.57	1.66
30	55.75	44.25	2.52

Table 1. Elemental composition of the products with different aluminizing time.

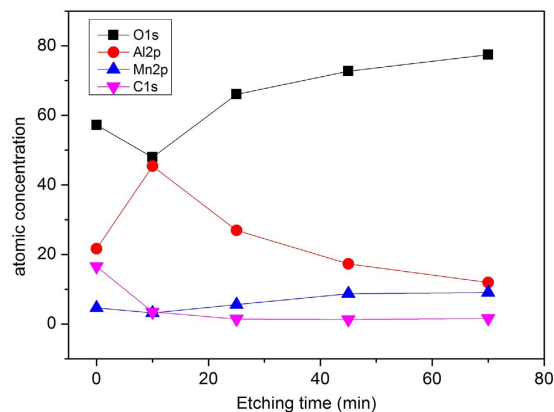
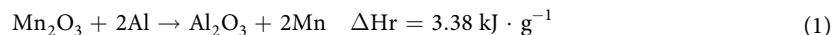


Figure 7. XPS depth profiling on atomic concentration within the $\text{Mn}_2\text{O}_3/\text{Al}$ membrane as a function of Ar^+ etching time.

In order to examine the elemental composition in the deeper layers within the nanothermite membrane, XPS depth profiling has been investigated with the aid of Ar^+ sputtering on $\text{Mn}_2\text{O}_3/\text{Al}$ membrane of aluminizing time of 30 min. The acceleration energy of ion beam is set to 3000 eV, corresponding to the etching rate of about $12 \text{ nm}\cdot\text{min}^{-1}$. A wide range survey, Mn2p and Al2p taken after each cycle of sputtering are shown in Figs S2–S4 in supporting information. Figure 7 shows calculated atomic percentage of the major elements displayed in XPS survey. The atomic percentage of Al goes to a maximum at an etching time of 10 min, which indicates that there is some excessive Al on the top of the membrane. With the increasing of etching time, the percentage of Al reduces while the percentage of Mn increases. However, even after 70 min etching, Al is still visible with a 12% atomic percentage in the membrane. One can easily conclude that Al has entered into the structure and coated the 3DOM Mn_2O_3 skeleton in three dimensions, which is also confirmed by TEM examination, see Fig. 5.

Energy release. The self-propagating reaction between Al and Mn_2O_3 would happen under the stimulus of flame, laser pulse, current, heating, etc. The reaction equation is described in the following equation (1),



The thermite reaction of $\text{Mn}_2\text{O}_3/\text{Al}$ nanothermite membrane is characterized with differential scanning calorimetry (DSC). The DSC curves from $\text{Mn}_2\text{O}_3/\text{Al}$ nanothermite membranes obtained with different aluminizing times are shown in Fig. 8. Only a small exothermic peak is arisen from the sample with aluminizing for 10 min in Fig. 8a, which indicates that Al is far from enough, in agreement with the molar ratio of Al to Mn_2O_3 is only 0.73 calculated by EDS. When the aluminizing time is added to 20 min, see Fig. 8b, there are two major exotherms, but most of energy is released in the first exotherm. The second exothermic reaction starts after the melting point of Al at 660°C . In addition, a weak endothermic peak is also observed. This is because the product of thermite reaction at interface prevent Al to react completely²¹. As shown in Fig. 8c, the larger endothermic peak reveals that there is excessive Al after the first exothermic reaction. The heat absorption capacity is $0.10 \text{ kJ}\cdot\text{g}^{-1}$. All these peaks are with sharp profile, which suggests the energy release in a short period of time. Therefore, it implies that the thermite reaction between Al and Mn_2O_3 can be divided into two steps. First reaction is based on solid-solid diffusion mechanism, and second reaction triggers by liquid-solid diffusion mechanism after Al is melted, which is similar to NiO/Al system that has been reported before³⁷. In comparison, the DSC curve of $\text{Mn}_2\text{O}_3/\text{Al}$ NPC under the same test conditions is shown in Fig. 8d. The profile of exothermic peak from NPC is similar to Fig. 8a, and the output of energy is just a little higher than $\text{Mn}_2\text{O}_3/\text{Al}$ membrane at aluminizing time of 10 min, which reveals that reactants are not able to react completely, although Al and Mn_2O_3 are mixed in the stoichiometric ratio.

In order to compare the influence of aluminizing time on the DSC results, all the experimental data are collectively listed in Table 2. It shows that total energy release has achieved its maximum, $2.09 \text{ kJ}\cdot\text{g}^{-1}$, when the aluminizing time is 30 min. Its first energy release is not the largest, but the second one is five times larger than that from the sample with 20 min aluminizing. This is owing to the excessive Al on the interface. On the other hand, Al is insufficient in the sample with aluminizing time of 20 min. We draw the conclusions that the first exothermic reaction is mainly controlled by the coverage of the fuel. When it's too thick, products cumulated on the interface may prevent the reaction to progress further, but the reaction is resumed after the residual Al is melted. Therefore, the total energy release is determined by the Al layer thickness deposited on the Mn_2O_3 skeleton. In addition, the maximum energy release is still lower than the theoretical value of $3.38 \text{ kJ}\cdot\text{g}^{-1}$, which may be attributed to the unavoidable oxidation of Al film during storage, and the fact that $\text{Mn}_2\text{O}_3/\text{Al}$ membrane is not in stoichiometric ratio. Despite all this, the energy release is still considerably high, and the first onset temperature is as low as 480°C , which is approximately 50°C lower than $\text{Mn}_2\text{O}_3/\text{Al}$ NPC. These characteristics make the $\text{Mn}_2\text{O}_3/\text{Al}$ nanothermite membrane a remarkable nanoenergetic material.

Figure 9 shows the corresponding XRD patterns of $\text{Mn}_2\text{O}_3/\text{Al}$ nanothermite membranes and $\text{Mn}_2\text{O}_3/\text{Al}$ NPC after DSC test. From the sample with aluminizing time of 10 min, in Fig. 9a, MnO (JCPDS 75-0626) peaks are observed without peaks from Al and Mn_2O_3 . This means that Al has reacted with Mn_2O_3 unreservedly during

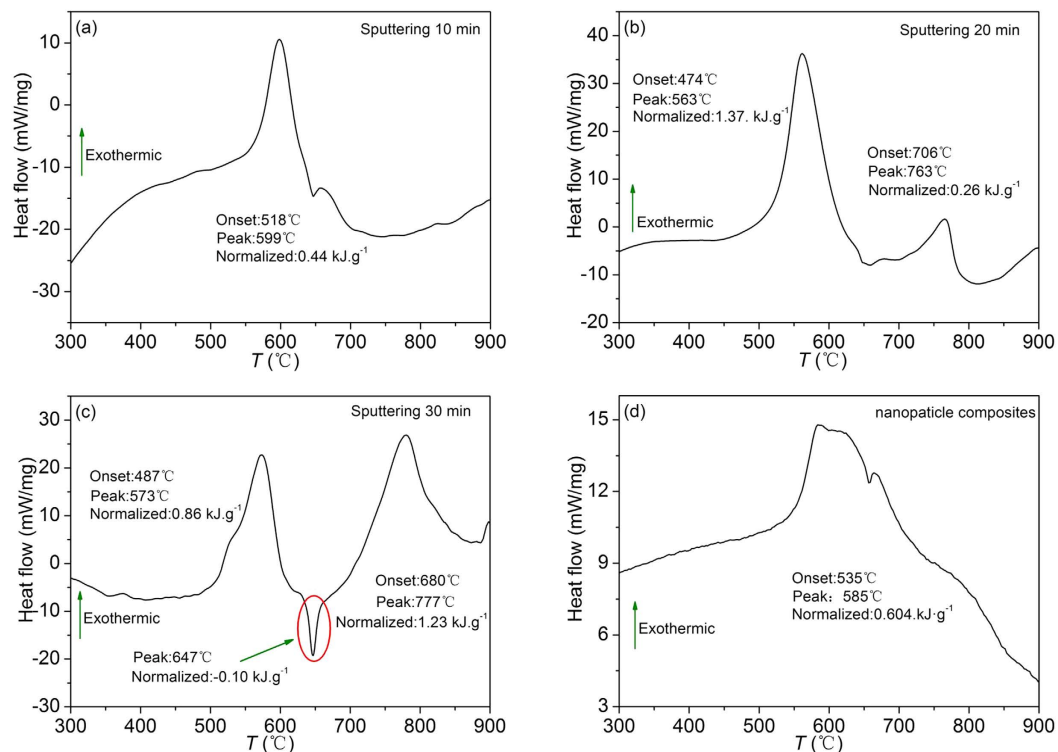
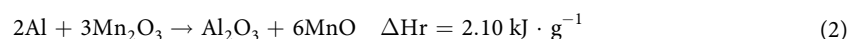


Figure 8. DSC curves of Mn₂O₃/Al membrane obtained in a temperature range from 200 to 900 °C with a heating rate of 20 °C·min⁻¹ under a 30.0 mL·min⁻¹ N₂ flow with different aluminizing times. (a) 10 min, (b) 20 min, (c) 30 min, and (d) DSC curve of Mn₂O₃/Al nanoparticle composites.

Aluminizing time (min)	First onset temperature (°C)	First energy release (kJ·g ⁻¹)	Second onset temperature (°C)	Second energy release (kJ·g ⁻¹)	Total energy release (kJ·g ⁻¹)
10	518	0.44	–	–	0.44
20	474	1.37	706	0.26	1.63
30	487	0.86	680	1.23	2.09

Table 2. DSC results analysis of Mn₂O₃/Al nanothermite membrane with different aluminizing time.

heating process, and Al is insufficient to reduce Mn₂O₃ thoroughly. The oxidation–reduction reaction is expressed in the following equation (2):



Similar pattern is obtained from the samples of Mn₂O₃/Al membrane with 20 min aluminizing, in Fig. 9b, and Mn₂O₃/Al NPC, in Fig. 9d. It is worth noting that the expected Al₂O₃ and Mn peaks are not presented. That is probably due to the product of Al₂O₃ and Mn are amorphous or nanocrystalline^{3,27,38}. The XRD pattern from the sample with aluminizing time of 30 min, in Fig. 9c, doesn't exhibit any characteristic peaks of MnO, which reveals that MnO has been reduced completely.

Laser Ignition Test. The ignition performance of 3DOM Mn₂O₃/Al nanothermite membrane has been tested with the sample of 30 min aluminizing. We assumed that one frame prior to the point of light appearing to be the initial time, and a sequence of test results with an interval of 20 μs between adjacent images are shown in Fig. 10. After a laser pulse struck upon Mn₂O₃/Al nanothermite membrane, a bright flash of white light surrounded by amaranthine glow burst out from the substrate at 20 μs, which indicated that the Mn₂O₃/Al membrane was ignited successfully. The whole ignition process lasted around 180 μs, and the maximum height of the flame was 8 mm at 20 μs. The high speed camera observations of ignition with other aluminizing time are shown in Fig. S5. As aluminizing time increased (from 10 minutes to 20 minutes, then to 30 minutes), the ignition duration also increased (100 μs, 140 μs, and 180 μs, respectively). The height of the flame gets higher and sparks became stronger. It can be concluded that the reaction between Al and Mn₂O₃ releases more energy along with

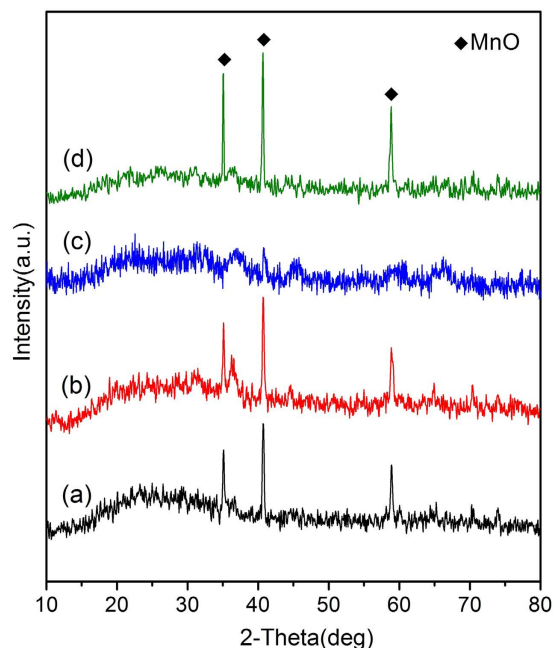


Figure 9. Corresponding XRD patterns of $\text{Mn}_2\text{O}_3/\text{Al}$ nanothermite membranes and $\text{Mn}_2\text{O}_3/\text{Al}$ nanoparticle composites after DSC test: (a) 10 min, (b) 20 min, (c) 30 min, and (d) $\text{Mn}_2\text{O}_3/\text{Al}$ nanoparticle composites.

the increasing of aluminizing time, which is consistent with the DSC results. It can be definitely concluded that a thermite reaction between Al and Mn_2O_3 occurred under the stimulus of laser pulse.

Summary

In this work, Mn_2O_3 is selected to combine with Al to achieve nanothermite of $\text{Mn}_2\text{O}_3/\text{Al}$. The 3DOM $\text{Mn}_2\text{O}_3/\text{Al}$ nanothermite membrane is prepared via a simple and feasible procedure: vertical deposition of CCT, inverse template method for 3DOM Mn_2O_3 skeleton and magnetron sputtering for $\text{Mn}_2\text{O}_3/\text{Al}$ nanothermite membrane. SEM results reveal that the Mn_2O_3 skeleton is highly ordered with interconnected and uniform macroporous structure, and Al is deposited uniformly onto the 3DOM Mn_2O_3 skeleton in order to form nanothermite membrane throughout the structure. With the increasing of aluminizing time, the Al layers get thickened. An optimized total energy release from nanothermite membrane of $2.09 \text{ kJ} \cdot \text{g}^{-1}$ with the onset temperature of around 480°C is achieved when the aluminizing time is increased to 30 min. In addition, laser ignition test results show a bright flash of light lasting up to $180 \mu\text{s}$. The 3DOM structural nanothermites possess the advantages of high energy density, large contact area, and short mass transfer distance that insure large energy release. Moreover, this method develops a new avenue to prepare various nanothermite membranes compatible with MEMS.

Methods

Fabrication of the 3DOM Mn_2O_3 skeleton. The PS spheres were synthesized by emulsifier-free polymerization technology in our laboratory³¹. The prepared PS spheres were assembled into a 3DOM CCT via vertical deposition method. In a typical procedure, an absolutely clean microslide substrate was vertically inserted into a spheres suspension (1.5 vol %), then, dried in the oven at a constant temperature of 50°C for 5 days. The number of CCT layers can be controlled by adjusting concentration of the PS suspension. Driven by a substrate–solution–air interface capillary action, PS spheres were deposited on the substrate gradually and in an orderly manner. 3DOM CCT was obtained when the solvent has evaporated completely. After that, the void space among the CCT was infiltrated with precursor and then removed to fabricate 3DOM metal oxides membrane. The selection of precursor is crucial. In this paper, $\text{Mn}(\text{Ac})_2 \cdot 4\text{H}_2\text{O}$ ($2.0 \text{ mol} \cdot \text{L}^{-1}$) was selected as the Mn source, which was dissolved in a mixture solution of methanol and ethylene glycol (volumetric ratio = 2/3). Simultaneously, moderate Polyvinyl Pyrrolidone (PVP) was added to increase the viscosity of the mixed solution. The influences of PVP on morphology are shown in Fig. S6 in the Supporting Information. After 12 hours of magnetic stirring, a magenta sol was formed and CCT was dipped into the prepared precursor vertically for 5 min. The residual liquid on substrate surface must be wiped off immediately once the template was lifted out of the precursor solution. The template filled with liquid precursor was then placed in an oven kept at 60°C for 4 hours to solidify the structure. At last, in order to remove the organic components the sample was calcined in a furnace with a heating rate of $1^\circ\text{C} \cdot \text{min}^{-1}$ and kept at 500°C for 1 hour in an open atmosphere.

Fabrication of the 3DOM $\text{Mn}_2\text{O}_3/\text{Al}$ nanothermite membrane. After the 3DOM Mn_2O_3 membrane was formed, Al was deposited onto the 3DOM Mn_2O_3 skeleton by magnetron sputtering to form core/shell structures with the 3DOM Mn_2O_3 as the core and Al as the shell. Prior to the Al deposition, the 3DOM Mn_2O_3 skeleton was rinsed by a small amount of anhydrous ethanol and dried under N_2 . All the sputtering process was under the vacuum condition of $5 \times 10^{-3} \text{ Pa}$, the DC voltage 150 V, and ultrahigh purity Ar as functional gas with the flux of

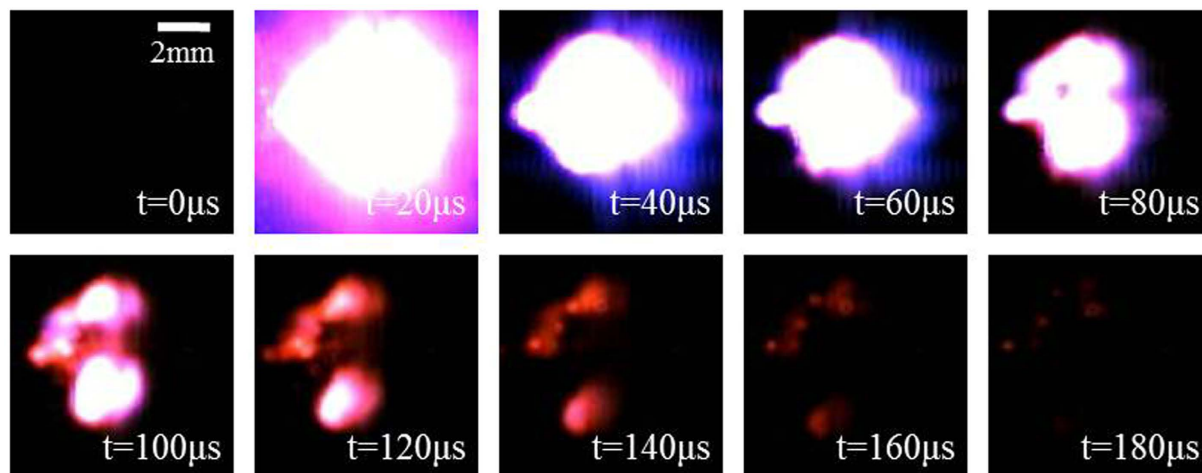


Figure 10. High speed camera observation of laser ignition test for $\text{Mn}_2\text{O}_3/\text{Al}$ nanothermite membrane with 30 min aluminizing time. The incident laser energy is 74 mJ per pulse.

30 sccm. On account of the high-vacuum and sustained low temperature, the oxidation of Al or the reaction of Mn_2O_3 and Al were mostly prevented during this process. In order to explore the influence of Al film thickness on the energy release from $\text{Mn}_2\text{O}_3/\text{Al}$ nanothermite membrane, various amounts of Al was deposited by varying the thickness of Al membrane, through controlling the aluminizing time. Three different aluminizing times were designed: 10 min, 20 min and 30 min, respectively.

For comparison purposes, $\text{Mn}_2\text{O}_3/\text{Al}$ NPC were also prepared via classic physical mixing. Aluminum particles with an average size of 50 nm were obtained from Aladdin Industrial Corporation (Shanghai, China), and Mn_2O_3 were purchased from Dk Nano Technology Corporation (Beijing, China). Stoichiometric mixtures of the reactants were separately mixed in hexane for 5 min in an ultrasonic bath and then added to one beaker for continuing ultrasonic dispersion for 30 min. The suspension was then moved to a vacuum oven kept at 70 °C under 1.5×10^4 Pa in order to obtain $\text{Mn}_2\text{O}_3/\text{Al}$ NPC.

Characterizations of samples. The morphology were characterized by a field-emission scanning electron microscope (FE-SEM) (Hitachi, S-4800) and a TEM (JEOL, JEM-2100). Elemental analysis of the 3DOM $\text{Mn}_2\text{O}_3/\text{Al}$ nanothermite membrane was carried out using EDS. XPS were taken using an ESCALAB250Xi XPS instrument (Thermo Scientific). A monochromatic Al K α x-ray source (1486.6 eV) was used with a spot size of 400 nm diameter. A pass energy of 100 eV and step size of 0.5 eV were used for survey spectra, and a pass energy of 20 eV and step size of 0.1 eV were used for high resolution spectra. Powder XRD (Bruker, D8Advance) was used to analyze the component of the material at each stage. Prior to the measurement, all the samples were striped from the microslide and attached onto a piece of flat quartz. In addition, the exothermic reaction of the 3DOM $\text{Mn}_2\text{O}_3/\text{Al}$ nanothermite membrane was performed by DSC (METTLER TOLEDO, DSC 1) under N_2 atmosphere in a temperature range of 200 to 900 °C with a flow rate of 30 mL·min⁻¹, and the heating rate was set to 20 °C·min⁻¹. A pulsed laser (Beamtech, DAWA-350) was used to investigate the ignition performance of the 3DOM $\text{Mn}_2\text{O}_3/\text{Al}$ nanothermite membrane. The laser was set to wavelength 1064 nm, pulse width 6 ns, beam diameter 700 μm , repetition rate 10 Hz, and the incident energy was 74 mJ per pulse. A piece of glass substrate with $\text{Mn}_2\text{O}_3/\text{Al}$ nanothermite membrane on it was placed at the focal point of the laser and a high speed camera was placed at a position perpendicular to the laser direction to observe the ignition process. The whole ignition process was recorded by a high speed camera (Redlake Motion Xtra, HG-100 K), and the data acquisition frequency was set as 50000 frames per second (fps).

References

- Chou, S. K., Yang, W. M., Chua, K. J., Li, J. & Zhang, K. L. Development of micro power generators – A review. *Appl. Energy* **88**, 1–16 (2011).
- Rossi, C. *et al.* Nanoenergetic materials for MEMS: a review. *J. Microelectromech. Syst.* **16**, 919–931 (2007).
- Dreizin, E. L. Metal-based reactive nanomaterials. *Prog. Energy Combust. Sci.* **35**, 141–167 (2009).
- Manesh, N. A., Basu, S. & Kumar, R. Experimental flame speed in multi-layered nano-energetic materials. *Combust. Flame* **157**, 476–480 (2010).
- Ohkura, Y., Liu, S.-Y., Rao, P. M. & Zheng, X. Synthesis and ignition of energetic CuO/Al core/shell nanowires. *Proc. Combust. Inst.* **33**, 1909–1915 (2011).
- Sullivan, K. & Zachariah, M. Simultaneous Pressure and Optical Measurements of Nanoaluminum Thermites: Investigating the Reaction Mechanism. *J. Propul. Power* **26**, 467–472 (2010).
- Jacob, R. J., Jian, G., Guerieri, P. M. & Zachariah, M. R. Energy release pathways in nanothermites follow through the condensed state. *Combust. Flame* **162**, 258–264 (2015).
- Zhu, P. *et al.* Energetic semiconductor bridge device incorporating Al/MoOx multilayer nanofilms and negative temperature coefficient thermistor chip. *J. Appl. Phys.* **115**, 194502 (2014).
- Zhang, K., Rossi, C., Petrantonio, M. & Mauran, N. A nano initiator realized by integrating Al/CuO-based nanoenergetic materials with a Au/Pt/Cr microheater. *J. Microelectromech. Syst.* **17**, 832–836 (2008).
- Staley, C. S. *et al.* Fast-Impulse Nanothermite Solid-Propellant Miniaturized Thrusters. *J. Propul. Power* **29**, 1400–1409 (2013).

11. Rossi, C., Estève, A. & Vashishta, P. Nanoscale energetic materials. *J. Phys. Chem. Solids* **71**, 57–58 (2010).
12. Jian, G., Liu, L. & Zachariah, M. R. Facile aerosol route to hollow CuO spheres and its superior performance as an oxidizer in nanoenergetic gas generators. *Adv. Funct. Mater.* **23**, 1341–1346 (2013).
13. Zhou, X., Torabi, M., Lu, J., Shen, R. & Zhang, K. Nanostructured Energetic Composites: Synthesis, Ignition/Combustion Modeling, and Applications. *ACS Appl. Mater. Interfaces* **6**, 3058–3074 (2014).
14. Wang, L., Luss, D. & Martirosyan, K. S. The behavior of nanothermite reaction based on Bi₂O₃/Al. *J. Appl. Phys.* **110**, 074311 (2011).
15. Wen, J. Z. *et al.* Characterization of thermochemical properties of Al nanoparticle and NiO nanowire composites. *Nanoscale Res. Lett.* **8**, 1–9 (2013).
16. Glavier, L. *et al.* Nanoenergetics as pressure generator for nontoxic impact primers: Comparison of Al/Bi₂O₃, Al/CuO, Al/MoO₃ nanothermites and Al/PTFE. *Combust. Flame* **162**, 1813–1820 (2015).
17. Gash, A. E. *et al.* Use of epoxides in the sol-gel synthesis of porous iron(III) oxide monoliths from Fe(III) salts. *Chem. Mater.* **13**, 999–1007 (2001).
18. Bezmelnitsyn, A. *et al.* Modified Nanoenergetic Composites with Tunable Combustion Characteristics for Propellant Applications. *Propellants Explos. Pyrotech.* **35**, 384–394 (2010).
19. Wang, H., Jian, G., Egan, G. C. & Zachariah, M. R. Assembly and reactive properties of Al/CuO based nanothermite microparticles. *Combust. Flame* **161**, 2203–2208 (2014).
20. Séverac, F., Alphonse, P., Estève, A., Bancaud, A. & Rossi, C. High-Energy Al/CuO Nanocomposites Obtained by DNA-Directed Assembly. *Adv. Funct. Mater.* **22**, 323–329 (2012).
21. Kim, S. H. & Zachariah, M. R. Enhancing the rate of energy release from nanoenergetic materials by electrostatically enhanced assembly. *Adv. Mater.* **16**, 1821–1825 (2004).
22. Kwon, J. *et al.* Interfacial chemistry in Al/CuO reactive nanomaterial and its role in exothermic reaction. *ACS Appl Mater Interfaces* **5**, 605–613 (2013).
23. Lanthony, C. *et al.* Elementary surface chemistry during CuO/Al nanolaminate-thermite synthesis: copper and oxygen deposition on aluminum (111) surfaces. *ACS Appl Mater Interfaces* **6**, 15086–15097 (2014).
24. Xu, D., Yang, Y., Cheng, H., Li, Y. Y. & Zhang, K. Integration of nano-Al with Co₃O₄ nanorods to realize high-exothermic core-shell nanoenergetic materials on a silicon substrate. *Combust. Flame* **159**, 2202–2209 (2012).
25. Petrantonio, M. *et al.* Multilayered Al/CuO thermite formation by reactive magnetron sputtering: Nano versus micro. *J. Appl. Phys.* **108**, 084323 (2010).
26. Blobaum, K. J., Reiss, M. E., Plitzko, J. M. & Weihs, T. P. Deposition and characterization of a self-propagating CuO_x/Al thermite reaction in a multilayer foil geometry. *J. Appl. Phys.* **94**, 2915–2922 (2003).
27. Blobaum, K. J. *et al.* Investigating the reaction path and growth kinetics in CuO_x/Al multilayer foils. *J. Appl. Phys.* **94**, 2923–2929 (2003).
28. Bahrami, M. *et al.* Magnetron Sputtered Al-CuO Nanolaminates: Effect of Stoichiometry and Layers Thickness on Energy Release and Burning Rate. *Propellants Explos. Pyrotech.* **39**, 365–373 (2014).
29. Fu, S. *et al.* Deposition and characterization of highly energetic Al/MoO_x multilayer nano-films. *Eur. Phys. J. Appl. Phys.* **64**, 30301 (2013).
30. Zhang, K., Rossi, C., Ardila Rodriguez, G. A., Tenailleau, C. & Alphonse, P. Development of a nano-Al/CuO based energetic material on silicon substrate. *Appl. Phys. Lett.* **91**, 113117 (2007).
31. Zhang, W. *et al.* Significantly enhanced energy output from 3D ordered macroporous structured Fe₂O₃/Al nanothermite film. *ACS Appl. Mater. Interfaces* **5**, 239–242 (2013).
32. Zheng, G. Q. *et al.* Preparation of Porous Core/Shell Structure Fe₂O₃/Al Nanothermite Membrane by Template Method. *J. Inorg. Mater.* **30**, 610–614 (2015).
33. Menon, L. *et al.* Ignition studies of Al/Fe[sub 2]O[sub 3] energetic nanocomposites. *Appl. Phys. Lett.* **84**, 4735 (2004).
34. Yan, H. W., Blanford, C. F., Holland, B. T., Smyrl, W. H. & Stein, A. General synthesis of periodic macroporous solids by templated salt precipitation and chemical conversion. *Chem. Mater.* **12**, 1134–1141 (2000).
35. Stein, A., Wilson, B. E. & Rudisill, S. G. Design and functionality of colloidal-crystal-templated materials—chemical applications of inverse opals. *Chem Soc Rev* **42**, 2763–2803 (2013).
36. Cheng, Z., Russel, W. B. & Chaikin, P. M. Controlled Growth of Hard-Sphere Colloidal Crystals. *Nature* **401**, 893–895 (1999).
37. Zhang, K. *et al.* Integrating Al with NiO nano honeycomb to realize an energetic material on silicon substrate. *Appl. Phys. A* **94**, 957–962 (2008).
38. Yang, Y. *et al.* Hierarchical MnO₂/SnO₂ heterostructures for a novel free-standing ternary thermite membrane. *Inorg. Chem.* **52**, 9449–9455 (2013).

Acknowledgements

This work was supported by National Natural Science Foundation of China (Grant 51576101), Chinese Postdoctoral Science Foundation (Grant 2012M511285), Natural Science Foundation of Jiangsu Province of China (Grant BK20141399), the Fundamental Research Funds for the Central Universities (Grant 30915012101) and the Priority Academic Program Development of Jiangsu Higher Education Institutions.

Author Contributions

W.Z. and Y.C. conceived and designed the experiments. G.Z. performed the experiments. R.S., J.Y. and Z.Q. helped the experiments and joined the discussions. G.Z., W.Z. and Y.C. wrote the paper. The manuscript was written through contributions of all authors. All authors have given approval to the final version of the manuscript.

Additional Information

Supplementary information accompanies this paper at <http://www.nature.com/srep>

Competing financial interests: The authors declare no competing financial interests.

How to cite this article: Zheng, G. *et al.* Three-dimensionally Ordered Macroporous Structure Enabled Nanothermite Membrane of Mn₂O₃/Al. *Sci. Rep.* **6**, 22588; doi: 10.1038/srep22588 (2016).



This work is licensed under a Creative Commons Attribution 4.0 International License. The images or other third party material in this article are included in the article's Creative Commons license, unless indicated otherwise in the credit line; if the material is not included under the Creative Commons license, users will need to obtain permission from the license holder to reproduce the material. To view a copy of this license, visit <http://creativecommons.org/licenses/by/4.0/>